Regular Article

Physics with NOvA: a half-time review

Peter Shanahan[1,a] , Patricia Vahle[2], and for the NOvA Collaboration

[1] Fermi National Accelerator Laboratory, Batavia, IL 60510, USA
[2] Department of Physics, William & Mary, Williamsburg, VA 23187, USA

Abstract The NOvA experiment has been collecting data in the NuMI neutrino beam since 2014. In this article we describe the rich physics program of the experiment, including long-baseline oscillation measurements, neutrino cross-section measurements, searches for phenomena beyond the standard three flavor oscillation paradigm, as well as astrophysical searches. Only half way through its expected run plan, NOvA will continue to explore exciting physics topics through 2026 and beyond.

1 Physics overview

Over the past 25 years, experiments have firmly established the existence of neutrino flavor oscillation phenomena [1–9], consistent with the picture that the neutrino flavor eigenstates of the weak interaction, ν_e, ν_μ, and ν_τ are related to the neutrino mass eigenstates ν_1, ν_2, and ν_3 by the Pontecorvo–Maki–Nakagawa–Sakata (PMNS) unitary mixing matrix. The PMNS matrix is parameterized in terms of three mixing angles, θ_{12}, θ_{23}, and θ_{13}, and a complex phase that allows for the possibility of charge-parity (CP) violation in neutrino oscillations [10–12]. Oscillations arise from the different time evolution of the phases of the three mass eigenstates, resulting in terms in the oscillation probability that depend on the ratio L/E of the distance traveled to energy of the neutrino, with a frequency that depends on the differences between the squared masses of neutrino mass states, Δm^2, and an amplitude that is a function of the mixing angles.

Current long-baseline experiments have L/E $\sim$ 500 km/GeV, meaning the oscillation probability is dominated by the larger of the two mass splittings $\Delta m^2_{32} \sim 2.5 \times 10^{-3}$ eV^2 characteristic of the oscillation of atmospheric neutrinos, with the addition of a much smaller effect for GeV-scale neutrinos at earth-bound baselines, driven by the smaller solar mass splitting $\Delta m^2_{21} \sim 7.5 \times 10^{-5}$ eV^2 [13]. The mass-squared splitting Δm^2_{21} and the absolute value of Δm^2_{32} are known to percent-level precision [14]. The mixing angles have been measured and are known to be large relative to the analogous angles of the CKM matrix of the quark sector.

Despite the successes of neutrino oscillation experiments, many compelling questions remain. It is not yet established if θ_{23} is in the lower octant (smaller than $\pi/4$), upper octant (greater than $\pi/4$), or maximal (exactly equal to $\pi/4$), corresponding respectively to a flavor composition of the ν_3 mass eigenstate that is more tau, more muon, or equal muon and tau, possibly indicating the existence of a previously unknown symmetry of nature. Moreover, it is still unknown whether the ν_3 state (which has the least electron flavor of the three) is the most massive or least massive, corresponding to a normal or inverted mass ordering or hierarchy, a question that has bearing on the prospects of neutrinoless double beta-decay experiments. It is also not known whether neutrinos violate charge-parity (CP) symmetry, potentially bearing on the origin of the baryon asymmetry of the universe [15,16], or whether there are neutrino interactions or states beyond those described by the Standard Model.

These key remaining questions associated with the physics of neutrino masses and mixing can be addressed with measurements of muon neutrino disappearance and electron neutrino appearance due to flavor oscillations over long baselines in matter. The leading term in the electron neutrino appearance probability is proportional to $\sin^2 \theta_{23}$, unlike the $\sin^2 2\theta_{23}$ dependence of the dominant term of the muon neutrino disappearance probability, giving sensitivity to the octant of θ_{23}. Sensitivity to the mass hierarchy comes from the presence of electrons in matter that gives rise, through a shift in the potential for the electron flavor, to a modification to the oscillation probability that is opposite for neutrino vs. antineutrinos and for a normal vs. inverted mass hierarchy [17,18]. Finally, interference between solar and atmospheric terms in the oscillation probability allows the CP-violating phase δ_{CP} to manifest, through a change in sign between matter and antimatter, as

[a] e-mail: shanahan@fnal.gov (corresponding author)

a difference between the electron neutrino appearance oscillation probability for neutrinos and antineutrinos.

2 The NOvA experiment

NOvA was conceived, following the successful launch of the MINOS [19] experiment with its original emphasis on muon neutrino disappearance, as an experiment that would leverage the investment made in the NuMI beamline with a design optimized for the measurement of the subdominant electron neutrino appearance. The detectors are highly active tracking calorimeters made from low atomic-number materials to facilitate the identification of electromagnetic showers and are placed approximately 14 mrad off the NuMI beam axis. At this angle, the dependence of the neutrino energy on parent pion energy in two-body decays is weak, resulting in a beam flux at energies well-matched to the first oscillation maximum at the NOvA baseline, while suppressing the flux of higher-energy neutrinos that are a source of ν_e backgrounds from neutral current interactions. The Far Detector is placed 810 km from the neutrino source to maximize the matter effect and therefore sensitivity to the neutrino mass hierarchy. The design of the experiment offers a range of other physics opportunities, including the capability to make unique contributions to the measurement of neutrino-nucleus scattering cross sections, searches for sterile neutrinos, and astroparticle physics studies.

2.1 The NuMI beam

The NuMI beam [20] is created from the extraction of 120 GeV protons from the Fermilab Main Injector onto a 2 interaction-length graphite target. Two pulsed magnetic horns focus the hadrons produced in the target into a 675 m long decay pipe filled with helium at slightly below atmospheric pressure. Hadrons that have not decayed are stopped downstream of the decay pipe in an absorber comprised of aluminum and steel. Muons and neutrinos enter a 240 m section of rock prior to reaching the Near Detector hall. The hadron and muon fluxes are monitored by ionization chambers upstream of the hadron absorber, and in 3 alcoves placed at the start of the rock, after 12 m of rock, and after 30 m of rock. Upgrades to the Fermilab accelerator complex for NOvA [21] included a re-purposing of the former antiproton Recycler to enable slip-stacking beam from the 8 GeV Booster into the Main Injector [22], an improved RF system in the Main Injector to decrease the cycle time from 2.2 to 1.33 s, and improvements to the target system to handle the design goal of 700 kW beam power.

The resulting neutrino flux at the Near Detector location is shown in Fig. 1 for both neutrino mode, in which the horn current polarity focuses positively charged hadrons, and antineutrino mode, in which the horns select negatively charged hadrons. The flux is peaked near 2 GeV, and over the range 1–5 GeV yields an event sample of 96% ν_μ for horns operated in neutrino mode, 83% $\bar{\nu}_\mu$ for antineutrino mode, and less than 1% ν_e and $\bar{\nu}_e$. The remainder are "wrong sign" muon neutrinos, antineutrinos in neutrino mode and neutrinos in antineutrino mode.

2.2 The NOvA detectors

The NOvA detectors are tracking calorimeters, composed of long cells of polyvinyl chloride (PVC) [23] containing liquid scintillator, arranged in alternating horizontal and vertical planes. The cells are 6.6 cm along the beam direction and 3.9 cm transverse to the beam, with 4.8 mm external and 3.3 mm internal walls.

The liquid scintillator [24] consists of approximately 95% mineral oil, 5% pseudocumene, and trace amounts other chemicals. Light is captured by a 0.7 mm-diameter wavelength-shifting fiber running the length of each cell in a loop, with both ends terminating at one of 32 pixels of an avalanche photodiode (APD). Custom front-end electronics sample the shaped APD output waveform at 2 MHz (8 MHz) for the Far (Near) Detector, providing a typical offline single-hit timing resolution of 20 ns or better at the Far Detector [25].

The fiducial volumes of the detectors are 63% scintillator by mass. The elemental composition of the scintillator and PVC by mass is dominated by 66.7% carbon, 16.1% chlorine, and 10.8% hydrogen. The approximately 6 planes per radiation-length allow for excellent separation of electromagnetic and hadronic activity.

The Far Detector, located 810 km from the NuMI target in Ash River, Minnesota, is 15 m × 15 m × 60 m with a mass of 14 kt. The main body of the Near Detector, located 100 m underground at a distance of 1 km from the target, is 3.8 m × 3.8 m × 12.8 m with a mass of 193 t, followed by a 3.8 m-wide by 2.5 m-high muon range stack consisting of 10 steel planes of 10 cm thickness interspersed with pairs of scintillator planes. The Far Detector, located on the surface with an overburden of 1.2 m of concrete and 15 cm of barite, is exposed to 130 kHz of cosmic-ray activity. The cosmic ray rate at the Near Detector is negligible in the context of beam neutrino interactions.

Data for calibration and non-beam physics channels is collected and a variety of data-driven triggers using real-time reconstruction algorithms run on data stored in an online buffer farm at each detector [26]. Beam events are collected in both detectors using a 550 μs time window centered on the 10 μs beam spill window, triggered by a signal derived from the accelerator controls system. The wide time window of data collection compared to the beam spill is used to sample cosmic-ray activity and noise under the precise detector conditions that apply to the beam data.

2.3 Neutrino interactions and event reconstruction in NOvA

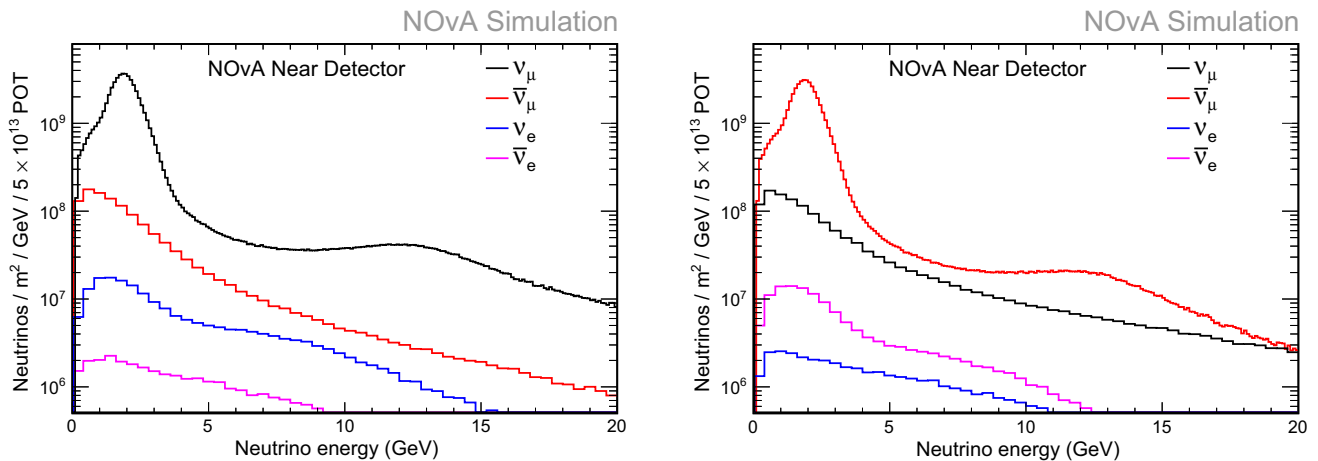Standard, three neutrino flavor oscillation studies require measurement of a neutrino's flavor and energy. Neu-

Fig. 1 The simulated beam flux at the NOvA Near Detector, for neutrino-mode (left) and antineutrino-mode (right) horn current polarity

trino flavor is determined through identification of the charged lepton produced in the final state of charged current (CC) interactions. Since the bulk of the NOvA flux is below the threshold for producing a tau, NOvA considers muon neutrino disappearance and electron neutrino appearance. Energy is determined calorimetrically for final state hadrons and electrons, or by range for muons. Figure 2 shows examples of a simulated muon neutrino CC interaction, an electron neutrino CC interaction, and a neutral current (NC) interaction in which the flavor of the interacting neutrino can not be determined.

In the 1–5 GeV energy range, CC interactions proceed through a number of different channels. At the low energies, the quasielastic (QE) channel dominates, in which the (anti)neutrino interacts with a neutron (proton) to produce a proton (neutron) and a $\mu^{-(+)}$ in the final state. As the neutrino energy increases and higher momentum transfers become possible, interactions involving production of pion-nucleon resonances (RES) and continuum pion production (DIS) become more significant. Additionally, as has become apparent in recent years [27,28], quasielastic-like scattering of neutrinos off correlated nucleon pairs (two-particle-two-hole or "2p2h"), is also an important component. Although the acceptance and energy reconstruction characteristics of these classes of interaction differ, the NOvA tracking calorimeter detector technology allows using all in the oscillation analyses.

Neutrino interactions in NOvA are simulated with a chain of software packages. The neutrino flux is modeled using G4NuMI, a GEANT based description of the NuMI beam line [29]. The raw flux from G4NuMI is then modified using the PPFX package to better match the products of the interactions in the extended target to the world's hadron production data [30]. Neutrino interactions and final state interactions are modeled using the GENIE neutrino interaction generator [31], while the final state particles are tracked using GEANT. Finally, a custom simulation models the light readout and front-end electronics response.

Pulses of light created when a charged particle traverses the scintillator are read out and digitized by the front-end electronics, and the time, location, and pulse-height of those signals are recorded as a hit. The variations in light output between cells and those due to attenuation along the readout fiber, in both data and simulation, are calibrated using cosmic-ray muons. The overall energy response of the detectors is calibrated using stopping muon tracks along a window from 200 to 100 cm before the end of the track. The absolute energy scale is cross-checked and benchmarked against simulation using beam-induced protons, muons, Michel electrons, and neutral pions at the Near Detector.

To reconstruct neutrino events, hits are first grouped in time and space into slices, each a cluster of hits likely correspond to the energy deposits from a single interaction. A slice is further analyzed to identify individual, final state particle tracks, called prongs. Flavor classification applies variants of convolutional neural networks, originally developed for computer vision applications, using all the hits in a slice as input. NOvA's implementation, named convolutional visual network (CVN), is trained on hit maps of simulated events to learn topological features that distinguish the flavors of neutrinos interacting in the detector [32].

The energy of charged current neutrino interactions is estimated from the sum of energies of the lepton and the hadronic recoil system. A Kalman-like algorithm is used with a BDT based on energy loss, multiple scattering, and length parameters of a candidate track to identify muons and reconstruct their energy using track length. The energy of electron neutrinos is estimated from a quadratic function, derived from the simulation, of the measured calorimetric energies of the electromagnetic activity and hadronic activity in the event [33,34].

2.4 NOvA status

NOvA started physics data-taking with the first 5 kt of the Far Detector in February 2014 and saw the completion of the Near and Far Detectors later that year.

Fig. 2 Example
simulated neutrino
interactions in the NOvA
Near Detector
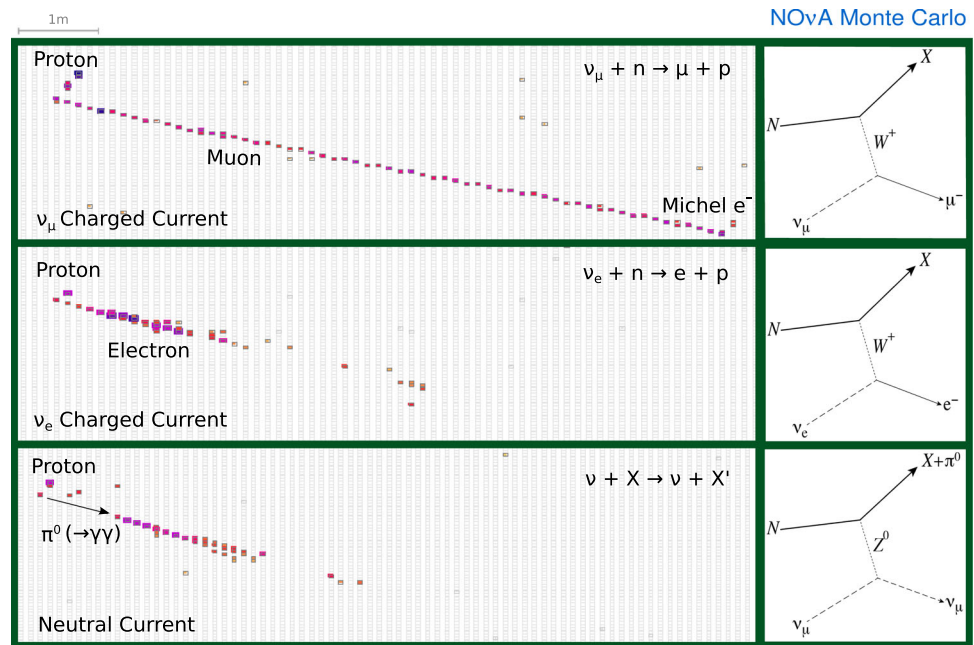
Annual beam exposure, measured in protons-on-target
(POT) to NuMI ramped up as the design beam power
for NOvA of 700 kW was achieved in 2017. Further
improvements to the NuMI target system now allow
even higher power, with a record 1 hour average power
of 843 kW. As of May 2021, the Far Detector has
recorded data for nearly 17×10^{20} POT delivered to
NuMI in neutrino mode and 12.7×10^{20} POT deliv-
ered in antineutrino mode. NOvA expects to continue
data-taking until 2026 and hopes to double the current
exposure in both neutrinos and antineutrinos.

3 Three-flavor oscillations

At the heart of the measurement of neutrino oscilla-
tions in NOvA is the prediction of the energy spectrum
and flavor composition of selected events in the Far
Detector for a given oscillation hypothesis. An *a pri-
ori* Far Detector prediction is subject to large system-
atic uncertainties. While the shape of the neutrino flux
spectrum is less uncertain at the NOvA off-axis loca-
tion than for the on-axis MINOS and MINERvA exper-
iments, hadron production uncertainties and uncertain-
ties in the modeling of the NuMI target and focusing
system combine to give an overall 10% uncertainty on
the flux normalization [35]. Neutrino-nucleus cross sec-
tions have typical uncertainties of 15–20%. Uncertain-
ties in the modeling of interactions of final-state parti-
cles in the detector can be non-negligible, particular for
neutrons, and the readout simulation model also con-
tributes uncertainties. However, virtually all of these
uncertainties are ameliorated by the two-detector tech-
nique, where data recorded in the Near Detector are
directly used to make a prediction of the event energy
spectrum and flavor composition in the Far Detector.

A full account of NOvA oscillation analyses are pre-
sented elsewhere [36–41] with the most recent results
presented in [42]; here, we focus on how the Near Detec-
tor data are used to constrain the prediction in the Far
Detector. The uses of observations in the Near Detec-
tor to improve the predicted spectra in the Far Detector
fall into two broad categories. In the first, physical or
effectively physical parameters in the models are tuned
to the muon charged current sample data. The second
category, called extrapolation, is a direct scaling of the
prediction at the Far Detector based on the remaining
differences between observation and tuned simulation
in the Near Detector in bins of relevant kinematic vari-
ables.

3.1 Cross-section model tune

Early comparisons of NOvA Near Detector data to
simulation showed substantial discrepancies in the
observed hadronic recoil energy distribution of selected
muon neutrino CC events. As seen in Fig. 3, the
comparison of the default simulation (using GENIE
version 2.12.2) to the NOvA data reveals a large
under-prediction of events in the region of of recon-
structed energy of the hadronic recoil system strad-
dling the QE-like and RES-like parts of the spectrum.
NOvA addressed this deficit using the optional empir-
ical meson-exchange current (MEC) model [43] avail-
able in GENIE 2.12.2 to represent the 2p2h process
of neutrino scattering from correlated nucleon pairs.
Informed by experience from MINERvA [27], that
empirical MEC model was further tuned, independently
for neutrino and antineutrino data, in bins of simulated
3-momentum transfer and energy transfer to match
NOvA Near Detector Data. Additional modifications
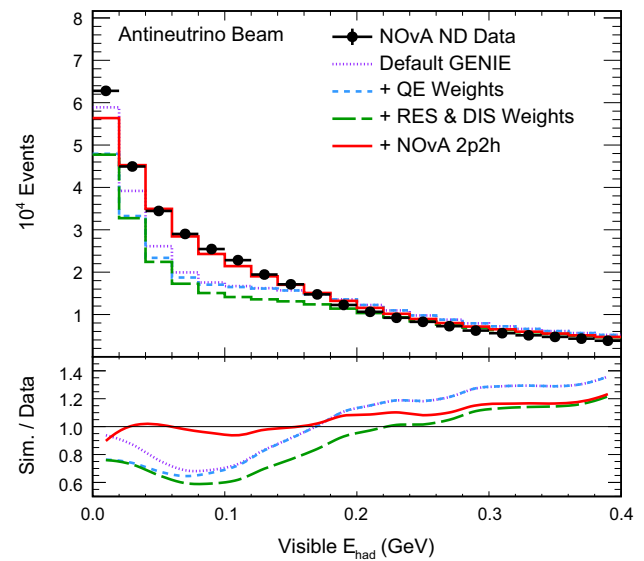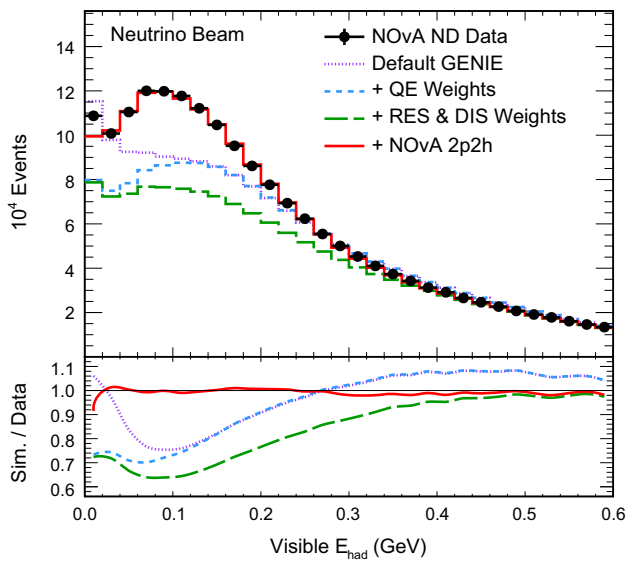to the default cross section model, motivated by exter-

Fig. 3 The reconstructed visible hadronic energy distribution for $\overset{(-)}{\nu}_{\mu}$ in the Near Detector for neutrino mode (left) and antineutrino mode (right), compared to the simulation at various stages of tuning of the cross-section model [44]

nal experimental constraints, were also applied. The full custom tune is described in [44].

For the NOvA oscillation results presented at Neutrino 2020 [42], the neutrino interaction model was updated to GENIE 3.0.6, which offers an expanded selection of models tuned to be compatible with existing data. Specifically, NOvA starts with the GENIE Comprehensive Model Configuration (CMC) G1810b_0211a, a theory-motivated set of models with parameter adjustments provided by GENIE. This configuration uses the quasi-elastic scattering model of the València group [45,46], the València MEC model [28] for scattering from correlated nucleon pairs, the model of Berger and Sehgal [47] for resonance production, and the Bodek–Yang model [48] for deep-inelastic scattering. Final state interactions (FSI) are handled in the semi-classical cascade hN treatment with a NOvA-custom adjustment for better agreement with external pion scattering data. NOvA also uses the z-expansion treatment of the axial form factor as examined in [49] for the evaluation of systematic uncertainties in the modeling of the QE channel.

Even with the updates to the GENIE models, data/Monte Carlo discrepancies remain, so the model is further tuned to match Near Detector data. The use of GENIE 3.0.6 allows for a simpler cross-section model tuning process than previous NOvA versions, in part due to more up-to-date tuning to data as part of the GENIE, and in part due to improvements in the selected models. For example, several improvements combine to remove the need for NOvA to apply an ad hoc suppression of resonance events at low values of Q^2. The València MEC model is adjusted using two independent two-dimensional Gaussians in the $(|\overrightarrow{q}|, q_0)$ space, reducing the number of MEC tuning parameters from 200 to 13. Moreover the modifications are the same for neutrino and antineutrino interactions. The comparison of data to the simulation is shown in

Fig. 4. Despite this reduction in complexity, the agreement between simulation and NOvA data is comparable to previous versions.

3.2 Extrapolation

Remaining discrepancies between Near Detector data and Monte Carlo are accounted for in the Far Detector prediction using a Far/Near extrapolation. The simulated event rate as a function of true neutrino energy is scaled to achieve perfect agreement with the observed spectra in the Near Detector. The same scaling in true energy is applied, along with the full 3-flavor disappearance oscillation probability in matter, to make the predicted muon (anti)neutrino Far Detector reconstructed energy spectrum. The predicted signal electron (anti)neutrino FD spectra are derived from the corrected FD muon neutrino spectrum with appearance oscillation probabilities applied.

Backgrounds to the electron neutrino appearance measurement are extrapolated using a Far/Near ratio in reconstructed energy. In neutrino mode, the electron neutrino selection is applied to the Near Detector, selecting a mixture of backgrounds from muon neutrino CC events with a high energy hadronic recoil system, neutral current (NC) events, and intrinsic beam electron neutrinos. Each of these background components has a different Far/Near ratio, so the contribution of each component is determined from data where possible [40]. Most of the intrinsic beam electron neutrino events come from the decay of muons produced with a muon neutrino, so the beam electron neutrino component is adjusted using the muon neutrino CC event spectrum recorded in the Near Detector. Once the beam electron neutrino component is determined, the distribution of the number of Michel electron candidates is used to further adjust the relative ratio of ν_μ CC and NC background events. In antineutrino mode, the back-
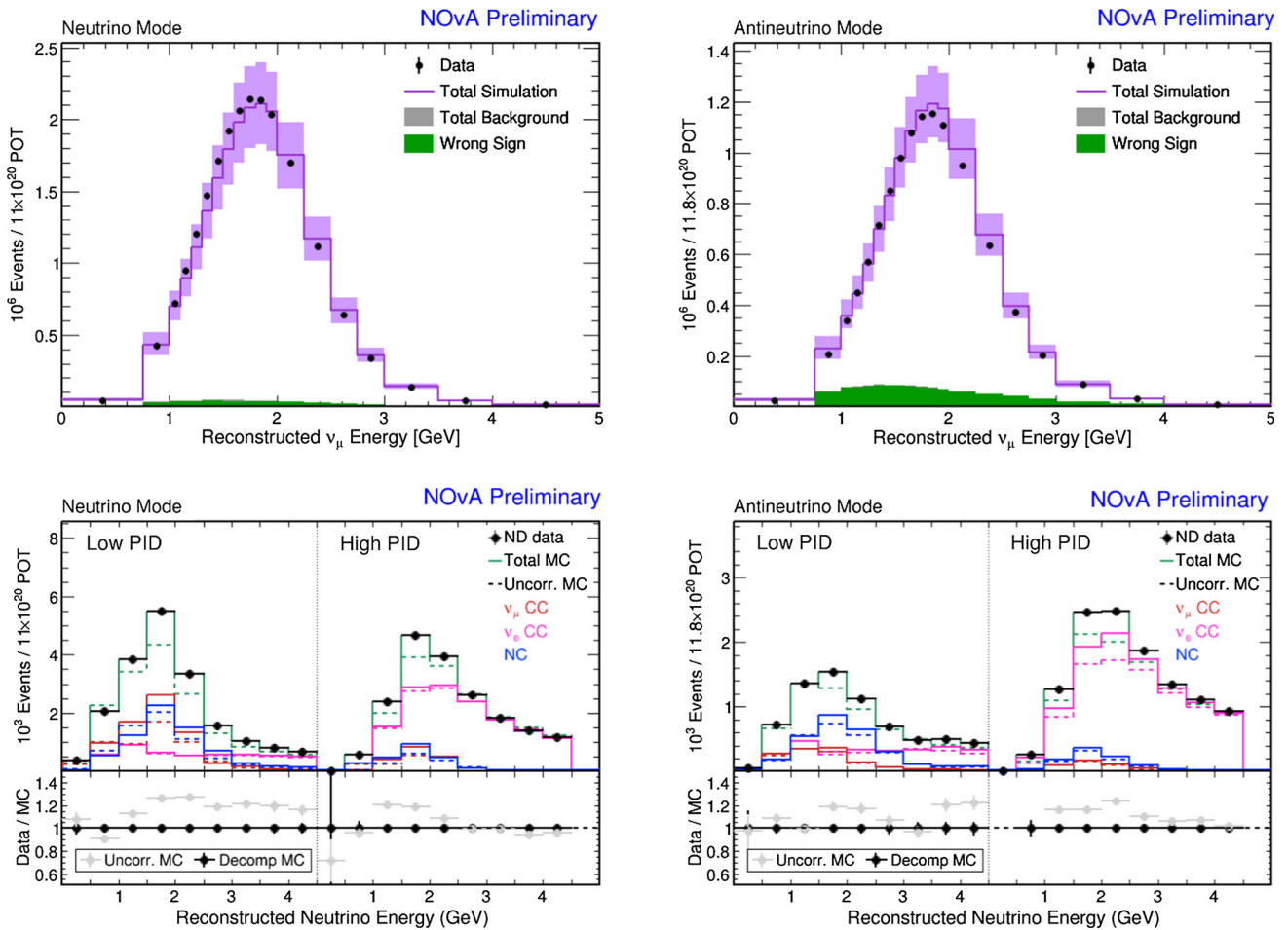
4264

Eur. Phys. J. Spec. Top. (2021) 230:4259–4273

Fig. 4 Observed spectra in the Near Detector, compared to result of the tuned simulation, for the $\overset{(-)}{\nu_\mu}$ samples (top), $\overset{(-)}{\nu_e}$ samples (bottom), for neutrino mode (left) and antineu-trino mode (right). The ν_μ histograms are absolutely normalized by protons-on-target, with the shaded area indicating the full uncertainty, dominated by flux normalization and cross-section modeling
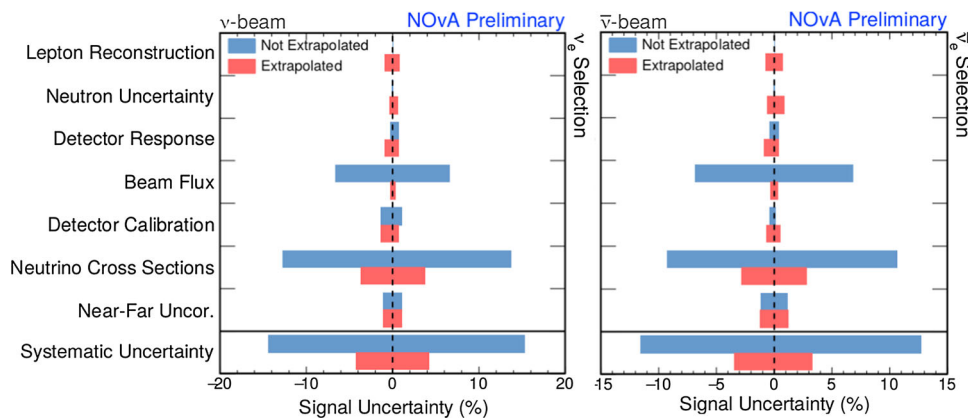

Fig. 5 The systematic uncertainties, grouped by major categories, on the ν_e signal in neutrino mode (left) and antineutrino mode (right). The red and blue bars indicate the uncertainty with and without the use of extrapolation, respectively. "Near-Far Uncor." includes effects like relative detector calibration that are not correlated between the two detectors
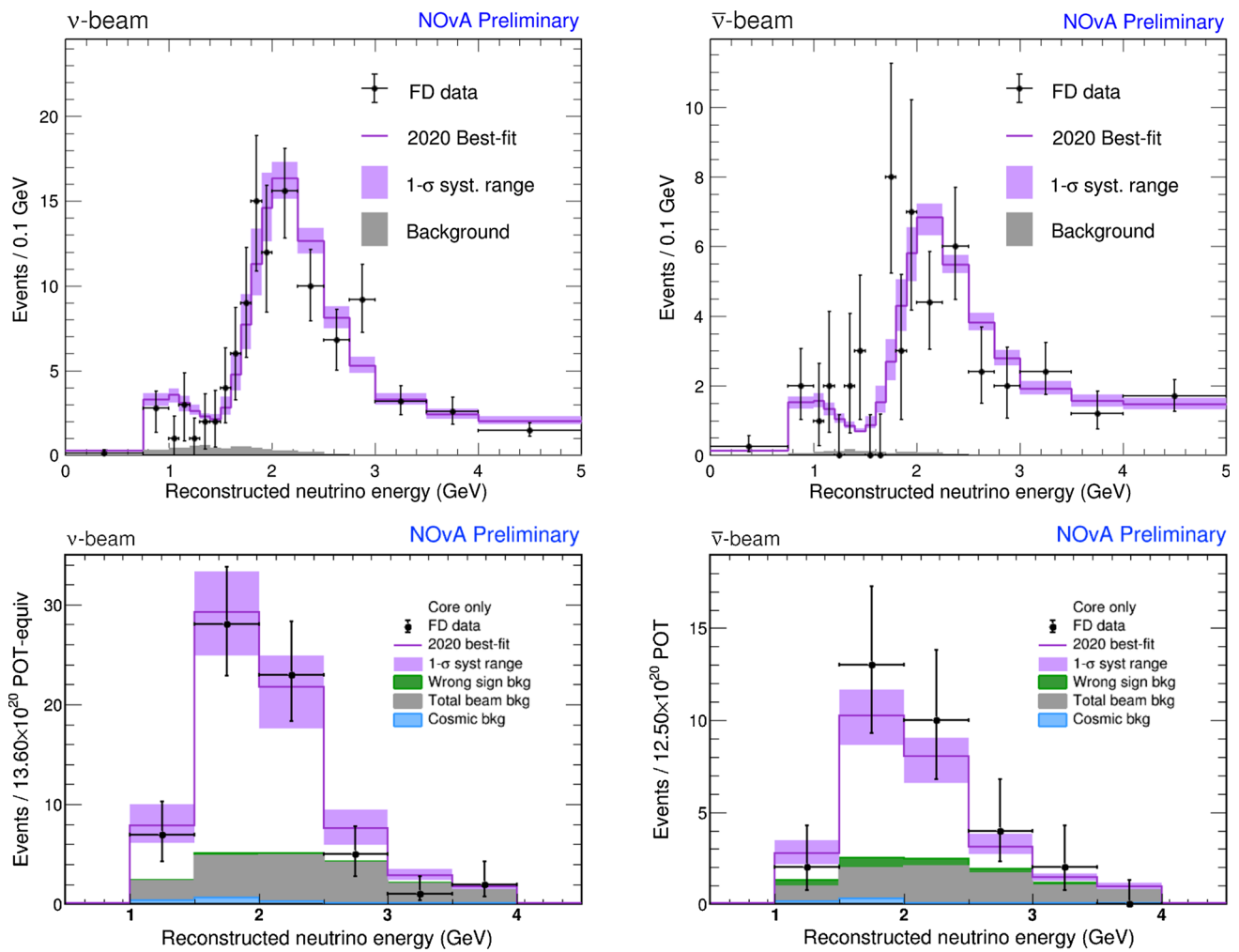
Fig. 6 Observed spectra in the Far Detector, compared to the prediction at the best fit point for oscillation parameters, for the $\overset{(-)}{\nu_\mu}$ samples (top), $\overset{(-)}{\nu_e}$ samples (bottom), for neutrino mode (left) and antineutrino mode (right). The sample of electron neutrino candidates near the edge of the detector that are used in the fit are not included in the plot

ground components are not decomposed using the data, but instead each component is scaled equally by the discrepancy between data and simulation in each bin of reconstructed energy. The lower panels of Fig. 4 show the comparison of selected electron neutrino events in the Near detector between data and simulation before and after the decomposition procedure.

A simple extrapolation procedure confers a degree of immunity from cross-section modeling uncertainties; however, acceptance and energy resolution differences among different interaction channels convoluted with the flux differences between the detectors (from both geometric effects and oscillations) and the size difference in the detectors give rise to residual systematic uncertainty in the Far Detector prediction. Two innovations in the extrapolation technique mitigate these effects in the NOvA oscillation analysis. Starting in 2018 [40], NOvA has applied the technique in bins of the fraction of reconstructed energy associated with the hadronic recoil system ("hadronic energy fraction") for muon neutrino interactions, bringing two benefits to

the analysis. First, given the difference in energy resolution for muons and hadronic activity in the NOvA detector, hadronic energy fraction is the main determinant of the energy resolution for a ν_μ CC interaction. The division of extrapolation by bins of hadronic energy fraction therefore allows the most accurately reconstructed events to have greater influence in the oscillation fit. Binning in hadronic energy fraction also tends to group interactions of similar physical processes together, further reducing the effect of neutrino cross-section modeling uncertainties by isolating classes of events with greater uncertainties. The second innovation, first applied in NOvA's 2020 result [42], has the extrapolation applied in bins of reconstructed transverse momentum (P_T) of the outgoing lepton. The narrower transverse dimensions of the Near Detector causes lower acceptance for higher-P_T events than for the Far Detector, leading to potential uncertainties associated with the modeling of the P_T-dependence of neutrino-nucleus cross sections. By applying the extrapolation separately in bins of P_T, the mismodeling is cor-

4266

Eur. Phys. J. Spec. Top. (2021) 230:4259–4273

rected by the Near Detector data. Figure 5 illustrates the effect of the extrapolation procedure on the size of the systematic uncertainty in the number of electron neutrinos and antineutrinos expected to appear at the Far Detector. A potential systematic uncertainty on the order of 15% is reduced to a 4-5% uncertainty.

3.3 Results

Once the prediction is established and systematic uncertainties are determined, oscillation parameters and their confidence intervals are estimated from a fit of the predicted muon neutrino and electron neutrino spectra, for neutrino and antineutrino beam modes, to the data in the Far Detector. The muon neutrino spectra are fit in bins of reconstructed hadronic energy fraction and neutrino energy. The electron neutrino spectra are fit in bins of reconstructed energy and electron-ID purity, thus enhancing the impact of the best-identified $\overset{(-)}{\nu_e}$ candidates. An additional sample of well-identified $\overset{(-)}{\nu_e}$ candidates occurring near the edge of the detector, and thus with poor energy reconstruction, is used without energy information. The values of oscillation parameters better constrained in other experiments—θ_{12}, θ_{13}, Δm_{21}^2—are taken from the PDG average [14]. Pull-terms representing systematic uncertainties are included in the fit. Figure 6 shows the Far Detector reconstructed energy spectra for neutrino and antineutrino, muon neutrino disappearance and electron neutrino appearance data compared to the prediction for the best fit values of oscillation parameters.

The NOvA data favor the normal mass hierarchy with $(\Delta m_{32}^2 = 2.41 \pm 0.07) \times 10^{-3} \text{eV}^2$, $\sin^2 \theta_{23} = 0.57^{+0.03}_{-0.04}$ and $\delta_{\text{CP}} = (0.82^{+0.27}_{-0.87})\pi$. Figure 7 shows the allowed regions of the oscillation parameters, where significance was determined using the unified approach of Feldman–Cousins [50]. The NOvA data do not show a strong asymmetry in the appearance of electron neutrinos as compared to electron antineutrinos and so disfavor combinations of oscillation parameters that lead to a strong asymmetry; the inverted mass hierarchy and $\delta_{\text{CP}} = \pi/2$ is disfavored at more than 3σ, while the normal mass hierarchy and $\delta_{\text{CP}} = 3\pi/2$ is disfavored at more than 2σ. The T2K experiment reports a larger asymmetry in the appearance of electron neutrinos compared to that measured in antineutrinos [51], giving rise to a mild tension.

4 Cross-section measurements in NOVA

While the multiple interaction channels and the lack of data underpinning neutrino cross-section models in the 1–3 GeV region [52] present a challenge for the oscillation measurement, it also represents an opportunity for NOvA. NOvA's excellent separation of electromagnetic and hadronic particles and good energy resolution for muons and electromagnetic showers, coupled with an intense, high-purity beam of either neutrinos or antineutrinos, allow NOvA to make compelling cross-section measurements.

### 4.1 ν_μ CC inclusive cross section

With millions of muon neutrino interactions in the Near Detector, NOvA is able to extract the ν_μ CC inclusive double-differential cross section in 172 bins of muon angle and energy. In addition to data quality, containment, and fiducial cuts, the heart of the selection for the ν_μ CC analysis is the presence of a highly muon-like, high-quality track. The muon identifier is a Boosted Decision Tree (BDT) using as input log-likelihood distributions in multiple scattering and energy deposition for the track as a whole, as well as variables characterizing the energy deposition near the end of the track. Since this analysis is not limited by statistics, the value of the cut on the muon identifier is chosen to minimize the systematic uncertainty on the cross section. The resulting sample of over 1 million candidate events is 86% pure ν_μ CC, with the background dominated by neutral current events.

The extraction of the double-differential cross section in bins of muon angle and energy requires correcting for the estimated background in reconstructed bins of these quantities, unfolding from reconstructed to true lepton kinematic quantities, and correcting for the selection efficiency of each true kinematic bin. These steps rely, respectively, on selection purity, an unfolding matrix, and selection efficiencies, which are derived from the tuned simulation. The overall selection efficiency and its dependence on the angle and energy of the muon differ strongly among the dominant processes contributing to the inclusive CC cross section in NOvA, because of the differing levels of hadronic activity. To limit the impact of uncertainties in the relative contributions and kinematic dependence of the QE, MEC, RES, and DIS in the simulation, the purity correction, unfolding, and efficiency correction are applied in three variables: lepton angle, lepton energy, and the summed energy of all observable hadrons in the event.

Systematic uncertainties are estimated by rerunning all steps of the analysis with a model that has been altered according to an underlying uncertainty, with a covariance matrix capturing the associated bin-to-bin correlations. The leading contribution of 9.1% to the total systematic uncertainty of 11.9% averaged across all bins is from the neutrino flux normalization uncertainty, while an average shape-only uncertainty of 8.1% is dominated by muon and hadronic energy scale uncertainties. The systematic uncertainty arising from neutrino interaction modeling averages to 1.5%. The average statistical uncertainty per bin is 1.8%.

Figure 8 shows the cross-section measurement in a sample of four muon-angle bins with comparison to the prediction of GENIE 2.12.2, with and without the NOvA tune. Unsurprisingly, the NOvA cross-section measurement agrees well with the NOvA tune based on GENIE 2.12.2. It also agrees well with the default GENIE 2.12.2 at higher angles, although at very for-

Fig. 7 The NOvA 1, 2 and 3 σ allowed range [42] in Δm^2_{32} vs. $\sin^2 \theta_{23}$ (left) and $\sin^2 \theta_{23}$ vs. δ_{CP} (right), for normal (top) and inverted (bottom) neutrino mass hierarchy. The NOvA best-fit point is indicated
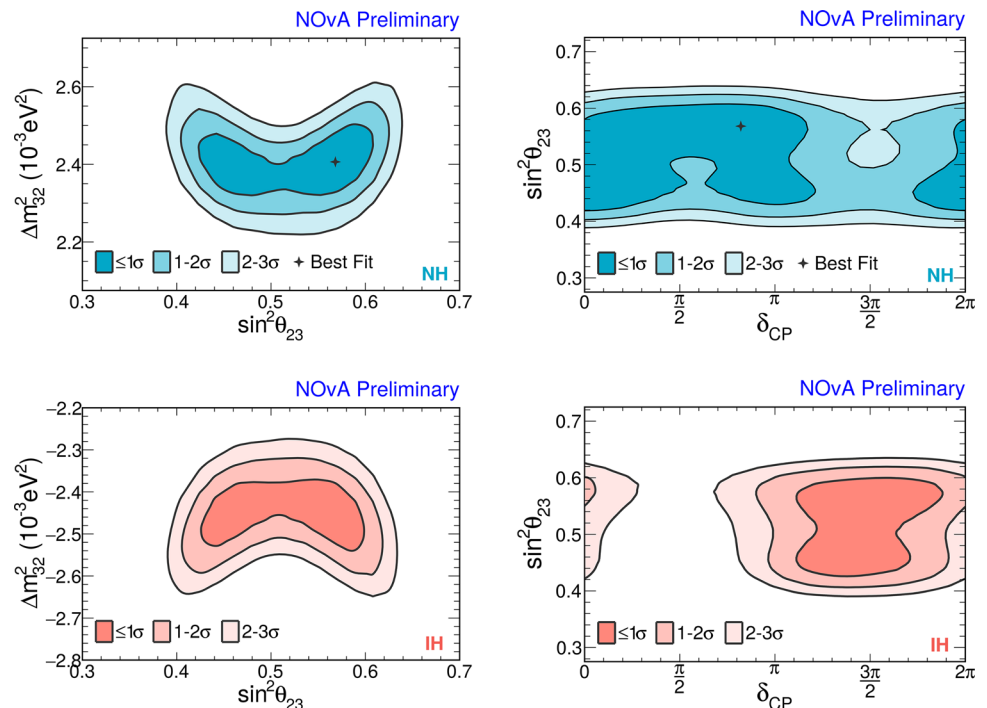
ward angles, corresponding to lower values of Q^2 populated by QE and MEC interactions, the data show a suppression of the cross section compared to the default GENIE 2.12.2 prediction. Full results can be found in [53], and will be published in an upcoming paper.

4.2 ν_e CC inclusive cross section

The approximately 1% level of the contribution of electron neutrinos to the NuMI flux at the NOvA Near Detector presents an additional challenge to the ν_e CC inclusive cross section. With the signal signature of an electron and possible additional activity from the hadronic recoil system, NC or ν_μ CC interactions with a final state containing photons from the decay of a π^0 are a potential major background. An event-level selection variable, ElectronID, is defined as the highest electron-like score of a prong-level BDT that takes as input the output of a convolutional neural network trained to distinguish electromagnetic and hadronic prongs, the width of a prong, and the distance of the starting position of the prong from the event vertex. Additional cuts are applied on data quality, containment of the event, vertex position, and to reject events with tracks that are likely associated with muons [54].

To provide a data-driven constraint on the significant remaining backgrounds, a fit of simulated ElectronID template distributions for signal and the dominant background processes is applied in bins of reconstructed electron energy and angle. The resulting signal distribution is then unfolded into the double-differential cross section in electron energy and angle.

Requirements that a bin contains at least 100 events, has a predicted signal-to-background ratio of 0.4 or greater, and that the background and signal templates

are sufficiently different, result in a cross-section measurement in 17 bins of E_e and $\cos(\theta_e)$, using 16,000 events containing a predicted 9961 ν_e candidates. Systematic uncertainties are evaluated in the same manner as for the ν_μ analysis. The leading contributions are the neutrino interaction model (9.8% bin-average relative uncertainty, weighted by measured cross section) and neutrino flux (9.1%), both of which are highly correlated among the bins of electron kinematics. The average statistical error is 7.4% per bin, with an overall average uncertainty of 18.1% per bin. The resulting preliminary flux-averaged cross section is shown in Fig. 9.

4.3 Neutral current coherent production of neutral pions

NOvA's spatial granularity enables a number of exclusive cross-section measurements. So far, the experiment has published a measurement of neutral-current coherent production of neutral pions ("NCCoh") [55]. This process results in the production of a π^0 while leaving the nucleus in the ground state. The signature for this channel is a single, forward π^0 in the final state, and no other significant hadronic activity. While this process accounts for roughly 1% of the total neutrino cross section in NOvA, the isolated electromagnetic shower can mimic an electron–neutrino interaction, making it an important process to model correctly.

In addition to basic data-quality cuts, the selection of the NCCoh sample requires the presence of exactly two reconstructed prongs, each classified as electromagnetic according to a likelihood-based particle ID algorithm, and little additional energy in the event. The invariant mass of the two-prong system is required to be consistent with a π^0 under the assumption that each is a

4268

Eur. Phys. J. Spec. Top. (2021) 230:4259–4273

Fig. 8 A sampling of the preliminary ν_μ CC inclusive cross section from NOvA [53], in bins of the cosine of the lepton scattering angle and energy, compared to default GENIE version 2.12.2 (dotted line) and the NOvA tune described in detail in [44] (solid line)
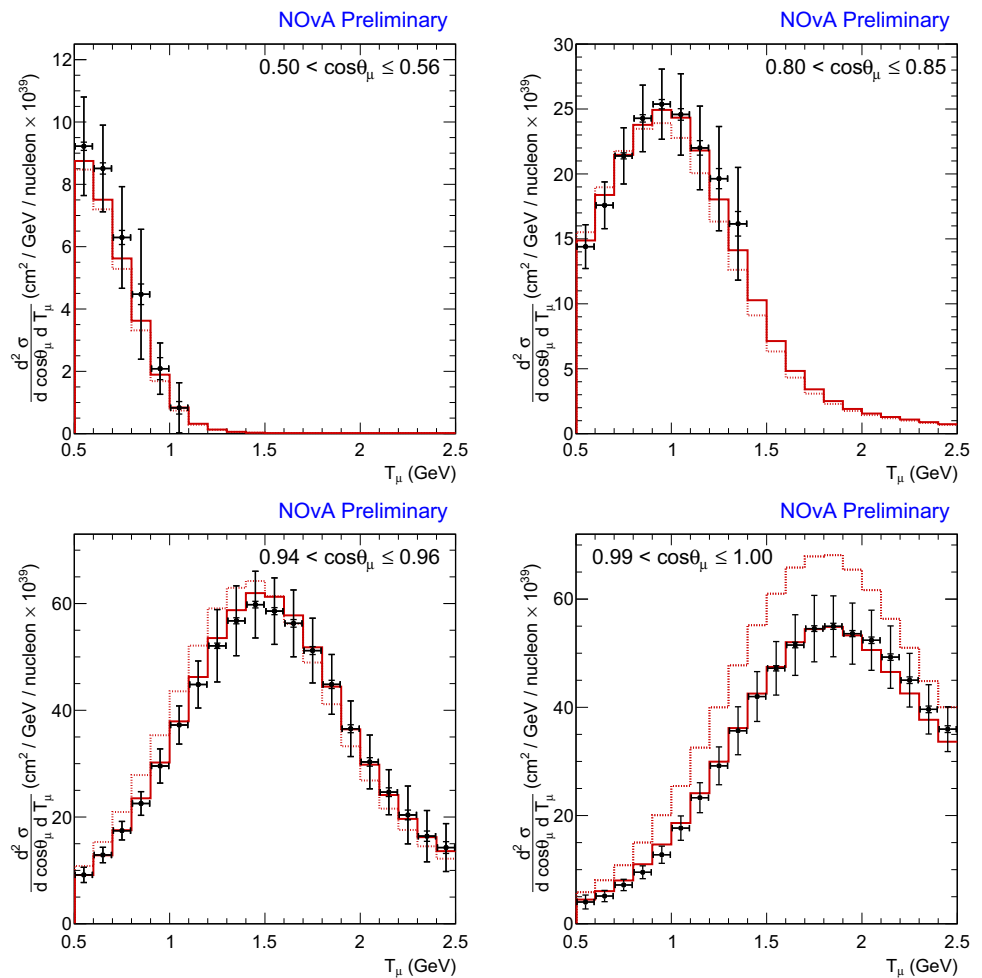
photon. An event-level convolutional neural network is used to further reject charged-current events. According to simulation, after these cuts, events with $\pi^0 s$ dominate the sample, although the majority are background resonance-production interactions.

A background-enhanced sample of events with more energy not associated with the pion is used to constrain these backgrounds and reduce the corresponding systematic uncertainty. The final signal-enhanced sample is defined as events with less than 10% of the energy not associated with the π^0, less than 0.3 GeV energy near the reconstructed event vertex, and events falling in bins of π^0 angle and energy that are predicted to have $> 15\%$ signal purity according to NOvA simulation using GENIE 2.10.4, where the coherent signal is simulated according to the model of Rein and Sehgal [56]. This final cut is chosen to reduce potential systematic uncertainties associated with observed discrepancies between data and the simulation in the pion angle.

The NOvA result, shown in Fig. 10, is the first measurement on a carbon-dominated target in the few-GeV region, and the most-precise measurement of the channel in this energy region to-date. The resulting measured cross section is $\sigma = 13.8 \pm 0.9(\text{stat.}) \pm 2.3(\text{syst.}) \times 10^{-40}$ cm^2/nucleus, with the systematic uncertainty dominated by modeling of the background (12.3% cross-section uncertainty) and neutrino flux (9.4%), in good agreement with the Rein-Sehgal model.

5 Non-standard neutrino phenomena

NOvA has significant reach in searches for phenomena induced by sterile neutrinos. A sterile neutrino does not participate in the electroweak interaction and has no corresponding charged lepton partner. In the standard 3-flavor picture, assuming unitarity and lepton universality, oscillations have no impact on the rate of neutral current interactions. Therefore, a comparison of the spectrum and rate of neutral current events between the NOvA Near and Far Detectors can be interpreted as a test for the effect of sterile neutrinos on oscillations. NOvA analyzes oscillations into a sterile state using the 3+1 model, in which a single sterile neutrino is added to the 3 active flavors. The 3+1 model admits 3 additional mixing angles, θ_{14}, θ_{24}, and θ_{34}, one new independent mass splitting Δm_{41}^2, and two new potentially CP-violating phases δ_{14} and δ_{24}.

The NOvA searches for NC disappearance that have been completed to-date apply to a mass splitting range

Fig. 9 The preliminary ν_e CC inclusive cross section from NOvA [53], in bins of the cosine of the lepton scattering angle and energy, compared to default GENIE version 2.12.2 (dotted line) and the NOvA tune described in detail in [44]
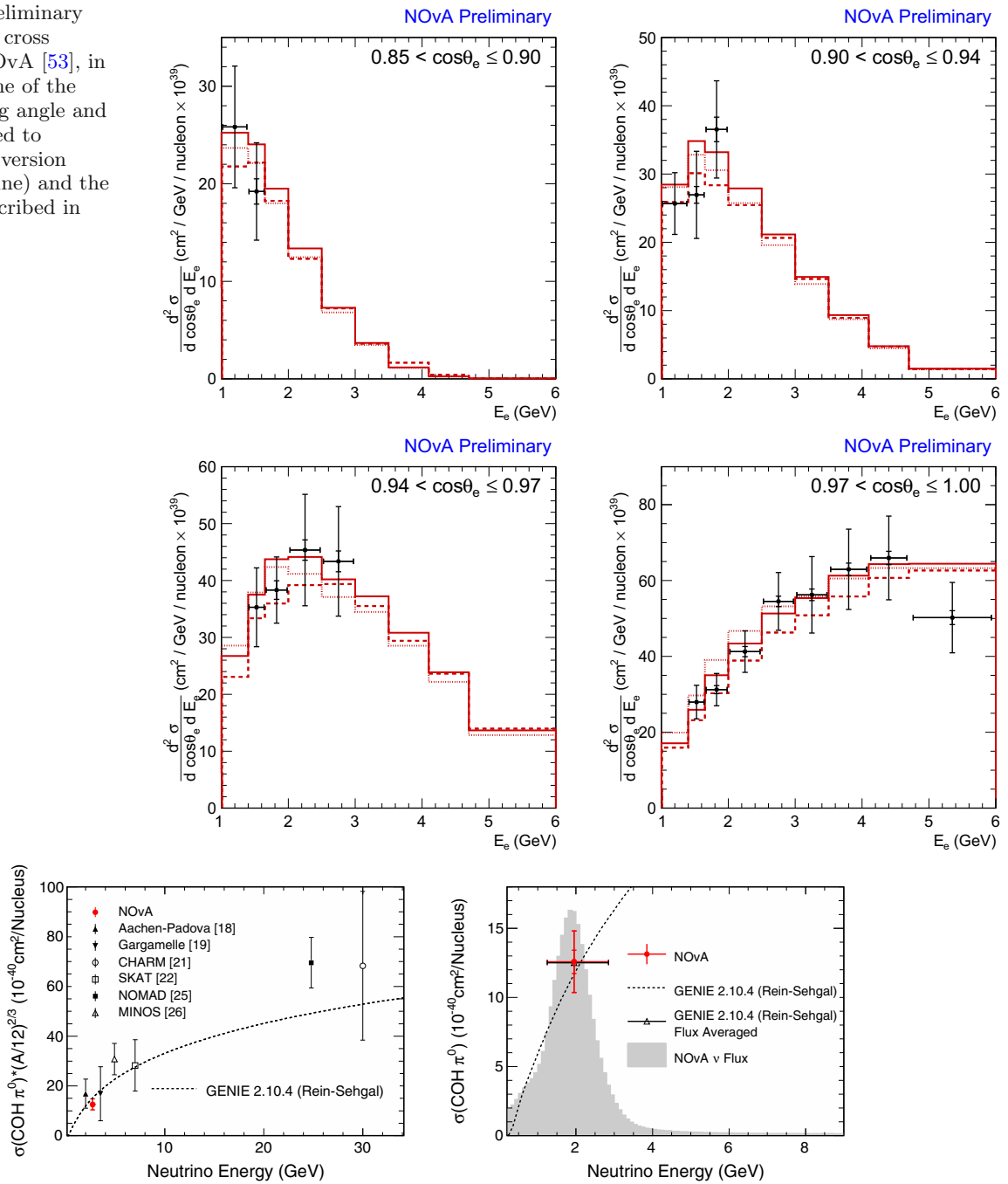

Fig. 10 The NOvA flux-averaged cross section [55] for $\nu_\mu + A \to \nu_\mu + A + \pi^0$. Left: the NOvA result compared to measurements of other experiments, each scaled to Carbon by the $(A/12)^{2/3}$ dependence following [57], and to

the Rein–Sehgal model [56]. Right: the NOvA measurement compared to the prediction from GENIE using the Rein–Sehgal model

of $0.05 < \Delta m^2_{41} < 0.5$ eV^2. Above this range, oscillations will affect the rate in the Near Detector, and below it degeneracy with the atmospheric-scale mass splitting Δm^2_{31} affects the interpretation of observations in the Far Detector. Among the new parameters of the 3+1 model, the NOvA analysis is sensitive to θ_{24}, θ_{34}, and δ_{24}.

In neutrino mode, NOvA observes 214 NC events in the Far Detector, compared to an expectation in the standard 3-flavor picture of 191 ± 14(stat.) ± 22(syst.) events [58]. In the first long-baseline, accelerator-based search for neutral current disappearance in an antineutrino-dominated beam, NOvA finds 121 events compared to the expectation of 122 ± 11(stat.)±15(syst), on a predicted background of 26 ± 3 events [59]. NOvA

4270

Eur. Phys. J. Spec. Top. (2021) 230:4259–4273

sees no significant suppression of neutral current interactions in either neutrino or antineutrino mode and sets limits on the mixing angles $\theta_{24} < 16.2°$ and $\theta_{34} < 29.8°$ for neutrinos and $\theta_{24} < 25°$ and $\theta_{34} < 32°$ for antineutrinos at the 90% C.L. for $0.05 < \Delta m^2_{41} < 0.5$ eV^2. Updates to the searches for evidence for the mixing of sterile and active neutrino flavors are in progress that will cover a greater range in Δm^2_{41}, with a covariance-matrix approach that considers potential signal manifest in both neutral and charged-current interactions.

6 Exotic phenomena, astroparticle, and cosmic ray physics

Beyond physics with neutrinos from the NuMI beam, NOvA studies seasonal variations of the cosmic ray muon rate, is able to detect neutrinos from core-collapse supernovae within our galaxy, and searches for a variety of exotic phenomena including magnetic monopoles and anomalous activity in time with gravitational wave alerts. NOvA publications on cosmic ray physics include measurements of the seasonal variation of the rate of multi-muon cosmic ray events at both the Near [60] and Far [61] Detectors. The measurements are in agreement with previous measurements [62] that show a peak rate of multi-muon events in the northern hemisphere winter. This effect is unexplained by current models and has the opposite seasonal effect observed in single-muon air showers.

The small overburden of the Far Detector, the large size of the detector, and the design of the trigger system combine to present NOvA with a niche sensitivity to cosmic-ray magnetic monopoles. Monopoles in the 10^8 GeV/c^2 mass range can penetrate the atmosphere and NOvA overburden, but would not penetrate to the MACRO experiment with its overburden of 3800 MWE. A selection optimized for monopoles of speed $\beta = 10^{-3}$ helps suppress potential backgrounds from cosmic-rays at the Far Detector, which tend to have speeds $\beta \sim 1$. With no events passing the selection criteria, NOvA sets an upper limit on the flux of monopoles in a region of mass-speed space that had not previously been constrained, $\phi < 2 \times 10^{-14}$ cm^{-2}s^{-1}sr^{-1} at 90% C.L. for $6 \times 10^{-4} < \beta < 5 \times 10^{-3}$ and mass greater than 5×10^8 GeV/c^2 [63].

Detailed observation of neutrinos from core-collapse supernovae will be key to understanding the physics process of the collapse and subsequent explosion [64] and may potentially contribute to our understanding of neutrino oscillation physics. While a single, few-MeV neutrino does not by itself induce much signal in the NOvA detectors, the enormous number of few-MeV neutrinos produced in a supernova triggers an impressive burst of activity, depending on distance to the supernova.

NOvA records potential supernova neutrino data from either detector in a self-triggering mode and also in response to a SNEWS alert [65]. With the significance threshold set to yield a background-induced trigger approximately once per week, the distance at which NOvA's trigger efficiency is estimated in the Garching model to be 50% is 6.2 kpc for a 9.6 $M_\odot$ star and 10.6 kpc for a 27 $M_\odot$ star [66]. Sensitivity to supernovae beyond 10 kpc is enabled by using SNEWS alerts to trigger readout of data held for 1350 s at the Far Detector and 1900 s at the Near Detector.

NOvA has also conducted searches for activity associated with the gravitational wave alerts issued by the LIGO/Virgo collaboration. A generic search using 28 such alerts found no significant excess over background [67]. A more recent search specifically targeting supernova-like signals excludes, found no unusual activity within 45 seconds of Far Detector data in coincident with 32 LIGO/Virgo alerts, which excludes at 90% CL the hypothesis that an alert was coincident with a 9.6 $M_\odot$ supernova in the Garching model within our galaxy [68].

7 NOvA outlook

NOvA is expected to take data through 2026 [69], when the Fermilab accelerator complex is shutdown for construction of the Long-Baseline Neutrino Facility (LBNF) for DUNE. During the remaining running time, the beam power delivered to NuMI should increase. Following installation of additional beam dampers and collimators scheduled as an early deliverable of the PIP-II project [70], the Fermilab accelerator complex should be capable of delivering more than 900 kW to NuMI. The ultimate exposure delivered to NuMI will depend on the timeline of the remaining power improvements, other demands on beam from the Main Injector, and the total run length. The current projection is between 60 and 70×10^{20} protons on target.

NOvA is currently in the midst of a test beam program at Fermilab using a 2.6 m $\times$ 2.6 m $\times$ 4.2 m detector, comprised of the same materials and technology as the Near and Far Detectors [71]. The accumulated samples of tagged charged pions, electrons, and protons with momenta between 0.5 GeV/c and 1.5 GeV/c, along with cosmic ray muons for calibration, will verify the response of the detectors to hadronic and electromagnetic activity and benchmark the simulation of single particle interactions in the detector.

In searches for exotic and other non-accelerator-neutrino topics [72], NOvA is exploring sensitivity to neutron-antineutron oscillations through the neutron annihilation signature. The magnetic monopole search is expected to remain background free through the end of NOvA data-taking. Searches for multimessenger neutrino signals coincident with gravitational wave alerts have the potential to gain in sensitivity due to planned expansions of the LIGO/Virgo/KAGRA [73] network. NOvA is investigating its sensitivity to dark matter candidates produced in the NuMI beamline or for neutrinos originating from dark matter annihilation in the sun [74,75].

NOvA's searches for sterile neutrinos and other non-standard neutrino phenomena continue [76], benefiting from further exposure and increased sophistication in analysis techniques. By the end of data-taking, NOvA is projected to have the strongest reach for sterile neutrino oscillation parameters among long-baseline experiments to-date, expanding the region of Δm^2_{41} and $\sin^2(\theta_{24})$ space currently excluded by MINOS, MINOS+, Daya Bay, and Bugey-3 [77]. In addition to sterile searches, NOvA is exploring searches for non-standard neutrino interactions in matter using ν_μ disappearance alone and combined analysis of ν_μ disappearance and ν_e appearance.

A broad range of cross-section measurements are underway within NOvA. Measurements of the $\bar{\nu}_\mu$ and $\bar{\nu}_e$ charged current inclusive cross sections will bring valuable information on antineutrino cross sections in an energy range where current data are extremely limited. Other measurements in progress include an analysis of a sample dominated by QE and MEC events through selection of single-track ν_μ CC events, analyses as functions of 3-momentum transfer and hadronic energy to further study the 2p2h process, and exclusive pion production channels with ν_μ and ν_e in both the neutrino and antineutrino beams [78]. Although the precision of NOvA cross-section results produced so far is limited by systematic uncertainties, increases in statistics will present opportunities to improve the granularity of measurements. Quadruple-differential measurements in lepton and hadronic recoil system kinematics will be possible in several channels, enabling a measurement of the ν_μ CC inclusive cross section reported in approximately 10,000 bins, the CC inclusive ν_e CC inclusive cross section in approximately 100 bins, semi-inclusive pion production channels, as well as double or single differential measurements in the very rare coherent pion production channels, respectively. Measurement of neutrino-electron and antineutrino-electron elastic scattering stands to address a leading systematic uncertainty of most NOvA cross-section measurements, by reducing the flux normalization uncertainty from around 10% to a few percent.

With the NOvA test beam effort underway and ongoing improvements to neutrino interaction measurements and modeling, the sensitivity of NOvA to three-flavor oscillation parameters will remain statistics-limited through the end of the experiment [79]. The expected total beam exposure will bring additional compelling milestones into reach. For the Mass Hierarchy, NOvA will achieve 95% a priori sensitivity for 40–60% of possible δ_{CP} values and 4–5σ a priori sensitivity for the most favorable combinations of the true values of the oscillation parameters. For CP-violation, a median, a priori sensitivity of 2-sigma is projected for 20–30% of the δ_{CP} range. The physics reach of NOvA will be complimented by a joint analysis effort underway between NOvA and T2K [80].

NOvA has already informed the design of the next generation of neutrino experiments from the insights gained from the performance of its beamline and detectors, and from its experience in operations and development of analysis techniques. NOvA has also informed the neutrino interaction and oscillation landscape with results from across its full portfolio of physics topics, and will continue to do so until the onset of the DUNE and T2HK era.

References

1. Y. Fukuda, T. Hayakawa, E. Ichihara, K. Inoue, K. Ishihara, H. Ishino, Y. Itow, T. Kajita, J. Kameda, S. Kasuga et al. (Super-Kamiokande Collaboration), Phys. Rev. Lett. **81**, 1562 (1998)

2. S. Fukuda, Y. Fukuda, M. Ishitsuka, Y. Itow, T. Kajita, J. Kameda, K. Kaneyuki, K. Kobayashi, Y. Koshio, M. Miura et al., Phys. Lett. B **539**, 179 (2002)

3. Q.R. Ahmad, R.C. Allen, T.C. Andersen, J.D. Anglin, J.C. Barton, E.W. Beier, M. Bercovitch, J. Bigu, S.D. Biller, R.A. Black et al. (SNO Collaboration), Phys. Rev. Lett. **89**, 011301 (2002)

4. K. Eguchi, S. Enomoto, K. Furuno, J. Goldman, H. Hanada, H. Ikeda, K. Ikeda, K. Inoue, K. Ishihara, W. Itoh et al. (KamLAND Collaboration), Phys. Rev. Lett. **90**, 021802 (2003)

5. D.G. Michael, P. Adamson, T. Alexopoulos, W.W.M. Allison, G.J. Alner, K. Anderson, C. Andreopoulos, M. Andrews, R. Andrews, K.E. Arms et al. (MINOS Collaboration), Phys. Rev. Lett. **97**, 191801 (2006)

6. K. Abe, N. Abgrall, Y. Ajima, H. Aihara, J.B. Albert, C. Andreopoulos, B. Andrieu, S. Aoki, O. Araoka, J. Argyriades et al. (T2K Collaboration), Phys. Rev. Lett. **107**, 041801 (2011)

7. Y. Abe, C. Aberle, T. Akiri, J.C. dos Anjos, F. Ardellier, A.F. Barbosa, A. Baxter, M. Bergevin, A. Bernstein, T.J.C. Bezerra et al. (Double Chooz Collaboration), Phys. Rev. Lett. **108**, 131801 (2012)

8. F.P. An, J.Z. Bai, A.B. Balantekin, H.R. Band, D. Beavis, W. Beriguete, M. Bishai, S. Blyth, K. Boddy, R.L. Brown et al., Phys. Rev. Lett. **108**, 171803 (2012)

9. J.K. Ahn, S. Chebotaryov, J.H. Choi, S. Choi, W. Choi, Y. Choi, H.I. Jang, J.S. Jang, E.J. Jeon, I.S. Jeong et al.

(RENO Collaboration), Phys. Rev. Lett. **108**, 191802 (2012)

10. B. Pontecorvo, JTEP **7**, 172 (1957)

11. V. Gribov, B. Pontecorvo, Phys. Lett. B **28**, 493 (1969)

12. Z. Maki, M. Nakagawa, S. Sakata, Prog. Theor. Phys. **28**, 870 (1962). https://academic.oup.com/ptp/article-pdf/28/5/870/5258750/28-5-870.pdf

13. H. Nunokawa, S.J. Parke, J.W.F. Valle, Prog. Part. Nucl. Phys. **60**, 338 (2008). arXiv:0710.0554

14. P.A. Zyla et al. (Particle Data Group), PTEP **2020**, 083C01 (2020)

15. E.K. Akhmedov, V.A. Rubakov, A.Y. Smirnov, Phys. Rev. Lett. **81**, 1359 (1998)

16. W. Buchmüller, R. Peccei, T. Yanagida, Annu. Rev. Nucl. Part. Sci. **55**, 311 (2005). https://doi.org/10.1146/annurev.nucl.55.090704.151558

17. L. Wolfenstein, Phys. Rev. D **17**, 2369 (1978)

18. S.P. Mikheyev, A.Y. Smirnov, Sov. J. Nucl. Phys. **42**, 913 (1985)

19. D.G. Michael et al. (MINOS), Phys. Rev. Lett. **97**, 191801 (2006). arXiv:hep-ex/607088

20. P. Adamson et al., Nucl. Instrum. Methods A **806**, 279 (2016). arXiv:1507.06690

21. D.S. Ayres et al. NOvA, The NOvA Technical Design Report, Report No. FERMILAB–DESIGN–2007–01 (2007). https://doi.org/10.2172/935497

22. R. Ainsworth, P. Adamson, B.C. Brown, D. Capista, K. Hazelwood, I. Kourbanis, D.K. Morris, M. Xiao, M.J. Yang, Phys. Rev. Accel. Beams **23**, 121002 (2020)

23. J.J. Grudzinski, R.L. Talaga, A. Pla-Dalmau, J.E. Fagan, C. Grozis, K. Kephart, R. Fischer (NOvA), J. Vinyl Additive Tech. **22**, 368 (2016)

24. S. Mufson et al., Nucl. Instrum. Methods A **799**, 1 (2015). arXiv:1504.04035

25. A. Norman, E. Niner, A. Habig, J. Phys. Conf. Ser. **664**, 082040 (2015)

26. A. Norman et al., J. Phys. Conf. Ser. **664**, 082041 (2015)

27. P.A. Rodrigues et al. (MINERvA Collaboration), Phys. Rev. Lett. **116**, 071802 (2016)

28. R. Gran, J. Nieves, F. Sanchez, M.J.V. Vacas, Phys. Rev. D **88**, 113007 (2013)

29. Z. Pavlovic. Ph.D. thesis, University of Texas (2008)

30. L. Aliaga et al. (MINERνA Collaboration), Phys. Rev. D **94**, 092005 (2016)

31. C. Andreopoulos et al., Nucl. Instrum. Methods A **614**, 87 (2010). arXiv:0905.2517

32. A. Aurisano, A. Radovic, D. Rocco, A. Himmel, M.D. Messier, E. Niner, G. Pawloski, F. Psihas, A. Sousa, P. Vahle, JINST **11**, P09001 (2016). arXiv:1604.01444

33. F. Psihas, Ph.D. thesis, Indiana U. (2018)

34. S. Yu, Ph.D. thesis, IIT, Chicago (2020)

35. L. Aliaga Soplin, Ph.D. thesis, William-Mary Coll. (2016)

36. P. Adamson et al. (NOvA), Phys. Rev. Lett. **116**, 151806 (2016). arXiv:1601.05022

37. P. Adamson et al. (NOvA), Phys. Rev. D **93**, 051104 (2016). arXiv:1601.05037

38. P. Adamson et al. (NOvA), Phys. Rev. Lett. **118**, 151802 (2017). arXiv:1701.05891

39. P. Adamson et al. (NOvA), Phys. Rev. Lett. **118**, 231801 (2017). arXiv:1703.03328

40. M.A. Acero et al. (NOvA), Phys. Rev. D **98**, 032012 (2018). arXiv:1806.00096

41. M.A. Acero et al. (NOvA), Phys. Rev. Lett. **123**, 151803 (2019). arXiv:1906.04907

42. M.A. Acero et al. (NOvA) (2021). arXiv:2108.08219

43. T. Katori, *Meson exchange current (MEC) models in neutrino interaction generators* (2013). arXiv:1304.6014

44. M.A. Acero et al. (NOvA, R. Group), Eur. Phys. J. C **80**, 1119 (2020). arXiv:2006.08727

45. J. Nieves, J.E. Amaro, M. Valverde, Phys. Rev. C **70**, 055503 (2004)

46. J. Nieves, J.E. Amaro, M. Valverde, Phys. Rev. C **72**, 019902 (2005)

47. C. Berger, L.M. Sehgal, Phys. Rev. D **76**, 113004 (2007). arXiv:0709.4378

48. A. Bodek, U.K. Yang, Modeling neutrino and electron scattering inelastic cross-sections in the few GeV region with effective LO PDFs TV leading order. In: 2nd International Workshop on Neutrino-Nucleus Interactions in the Few GeV Region. (2003). arXiv:hep-ex/0308007

49. A.S. Meyer, M. Betancourt, R. Gran, R.J. Hill, Phys. Rev. D **93**, 113015 (2016)

50. G.J. Feldman, R.D. Cousins, Phys. Rev. D **57**, 3873 (1998). arXiv:physics/9711021

51. K. Abe et al. (T2K), Phys. Rev. D **103**, 112008 (2021). arXiv:2101.03779

52. J.A. Formaggio, G.P. Zeller, Rev. Mod. Phys. **84**, 1307 (2012). arXiv:1305.7513

53. L. Cremonesi, Cross-section measurements with nova. (2020). https://doi.org/10.5281/zenodo.4155399

54. M.A. Judah, Ph.D. thesis, Colorado State U., Fort Collins (2019)

55. M.A. Acero et al. (NOvA), Phys. Rev. D **102**, 012004 (2020). arXiv:1902.00558

56. D. Rein, L.M. Sehgal, Nucl. Phys. B **223**, 29 (1983)

57. C. Berger, L.M. Sehgal, Phys. Rev. D **79**, 053003 (2009). arXiv:0812.2653

58. G.S. Davies (NOvA), PoS **NuFact2017**, 006 (2018)

59. M.A. Acero et al. (NOvA) (2021). arXiv:2106.04673

60. M.A. Acero et al. (NOvA), Phys. Rev. D **99**, 122004 (2019). arXiv:1904.12975

61. M.A. Acero et al. (NOvA) (2021). arXiv:2105.03848

62. P. Adamson, I. Anghel, A. Aurisano, G. Barr, M. Bishai, A. Blake, G.J. Bock, D. Bogert, S.V. Cao, C.M. Castromonte et al. (MINOS Collaboration), Phys. Rev. D **91**, 112006 (2015)

63. M.A. Acero et al. (NOvA), Phys. Rev. D **103**, 012007 (2021). arXiv:2009.04867

64. A. Mirizzi, I. Tamborra, H. Janka, N. Saviano, K. Scholberg, R. Bollig, L. Hudepohl, S. Chakraborty, Riv. Nuevo. Cim. **39**, 1 (2016)

65. P. Antonioli, R.T. Fienberg, F. Fleurot, Y. Fukuda, W. Fulgione, A. Habig, J. Heise, A.B. McDonald, C. Mills, T. Namba et al., New J. Phys. **6**, 114 (2004)

66. M.A. Acero et al. (NOvA), JCAP **10**, 014 (2020). arXiv:2005.07155

67. M.A. Acero et al. (NOvA), Phys. Rev. D **101**, 112006 (2020). arXiv:2001.07240

68. M.A. Acero et al. (NOvA) (2021). arXiv:2106.06035

69. P. Shanahan, P. Vahle, Snowmass 2021 Letters of Interest **NF**, 135 (2021)

70. M. Ball et al. The PIP-II Conceptual Design Report, ed. by V. Lebedev. Report No. FERMILAB–DESIGN–2017–01, FERMILAB–TM–2649–AD–APC (2017). https://doi.org/10.2172/1346823

71. M. Wallbank (NOvA), PoS **ICHEP2020**, 188 (2021)
72. A. Habig, O. Samoylov, M. Strait, Snowmass 2021 Letters of Interest **NF**, 217 (2021)
73. B.P. Abbott et al., Living Rev. Rel. **21**, 3 (2018)
74. W.H. Press, D.N. Spergel, Astrophys. J. **296**, 679 (1985)
75. T.K. Gaisser, G. Steigman, S. Tilav, Phys. Rev. D **34**, 2206 (1986)
76. A. Aurisano, G. Davies, B. Rebel, Snowmass 2021 Letters of Interest **NF**, 157 (2021)
77. P. Adamson, F.P. An, I. Anghel, A. Aurisano, A.B. Balantekin, H.R. Band, G. Barr, M. Bishai, A. Blake, S. Blyth et al. (Daya Bay Collaboration and MINOS+ Collaboration), Phys. Rev. Lett. **125**, 071801 (2020)
78. L. Cremonesi, M. Muether, J. Paley, Snowmass 2021 Letters of Interest **NF**, 264 (2021)
79. M. Baird, R. Nichol, L. Suter, J. Wolcott, Snowmass 2021 Letters of Interest **NF**, 133 (2021)
80. R. Patterson, M. Sanchez, S. Bolognesi, M. Hartz, K. Mahn, Snowmass 2021 Letters of Interest **NF**, 124 (2021)